Reflected Electro-Material Signatures for Self-Sensing Passive RFID Sensors

Azhar Hasan
Email: azhar.hasan@gatech.edu

Andrew F. Peterson
Email: peterson@ece.gatech.edu

Gregory D. Durgin
Email: durgin@gatech.edu

School of Electrical and Computer Engineering
Georgia Institute of Technology
Atlanta, Georgia 30332–0250

***Abstract*—In this paper, we evaluate realizations for implementing an RFID reflected electro-material signature (REMS) sensor. REMS sensors allow passive measurement, recording, and reading of environmental data such as temperature in a small, low cost device. This paper presents results from two configurations: a three-section lossless microstrip transmission line and a monopole probe inserted into a lossy medium. A neural network is used to recover the permittivity profile in either case, based on the reflection coefficient of the wave backscattered from an RF tag. The neural network incorporating the Levenberg Marquardt back-propagation algorithm is evaluated in terms of average error, regression analysis and computational efficiency in the presence of realistic noise. A unique contribution of this paper is the exploration of REMS using a dissipative electro-material medium. In the lossy case, two real-valued neural networks are integrated together to reconstruct the complex permittivity from the measured reflection coefficient. The approach is verified over the frequency range 4.0 - 5.0 GHz and less than 4% error was observed in presence of white Gaussian noise with 10dB SNR.**

I. Introduction

Wireless sensing is gaining interest from a wide variety of disciplines. Passive sensors, reducing cost and eliminating the life dependency on batteries, are obviously the preferred option. Advances in passive RFID sensors and recent developments in materials allow a number of tracking and sensing applications. As an example, capacitive peak strain sensors, using two concentric conducting pipes with dielectric in between, have been developed to monitor the structural health of materials [1]. The relative displacement of the pipes can be gauged through the change in capacitance, which causes a resonant frequency shift detectable by the RFID sensor. A second example is that of a corrosion sensor, which exploits the shift in resonant frequency as the length of the sensor wire changes, to sense the corrosion thresholds [2]. In the recent past researchers have also proposed single walled nanotube based inductively coupled passive wireless sensors for structural monitoring [3].

With recent advances in passive sensing, there is interest in sensors capable of monitoring variables over time in material or food supply chains. For example, when perishable goods are transported though cold supply chains and are exposed to temperature fluctuations, it results in reduced shelf life or quality degradation. One way of verifying that refrigerated food has been maintained at an appropriate temperature during storage and shipping is through the use of an RFID-based reflected electro-material signature (REMS) sensor, described below. REMS sensors are similar in concept to structural health monitors.

In our proposed system, the REMS sensor is a passive RF tag, which provides information through its input impedance. The input impedance of an RF tag is dependent on the physical/material properties of the tag, and this can be exploited to estimate the tag's permittivity using the multiport tag concept [4], [5]. Based on the fact that the RFID tag performance deteriorates in close vicinity of metals, Bhattacharyya et. al. proposed a RFID-tag-antenna-based sensor for temperature thresholds and displacement sensing [6]. They have also highlighted the concept of non-electronic memory in terms of recording the occurrence of an event in past: the event has occurred or not.

A REMS sensor must incorporate materials whose permittivity parameters can change significantly with environmental conditions [7]. A simple REMS sensor consists of an antenna attached to a microstrip transmission line, which in turn is routed over one or more sections of variable permittivity material before being terminated in a load. The environmental variables are recorded in the permittivity profile of the variable permittivity material, which can be in principle extracted from the backscattered wave. This is a form of the classical one-dimensional inverse scattering problem. For profile inversion in a lossy inhomogeneous media, analytical techniques are difficult to implement in most practical situations, and thus various numerical techniques have been investigated [8]. Researchers have explored methods such as the finite difference time domain technique [9] and 1-port and 2-port measurements [10] for extracting the material properties using the reflection/transmission methods. Artificial neural networks have been employed across a wide field of applications, including RF and microwave design [11], [12]; and inverse electromagnetic problems [13], [14], [15], and [16]. Neural networks are gaining popularity for material science based research as well, and are particularly suited to non-linear inverse profiling problems [17]. In this paper we propose a neural network based methodology for passive REMS sensing.

The REMS sensing concept is explained in the following section. A brief introduction to neural networks is given in

978-1-4244-9606-8/11/$26.00 ©2011 IEEE

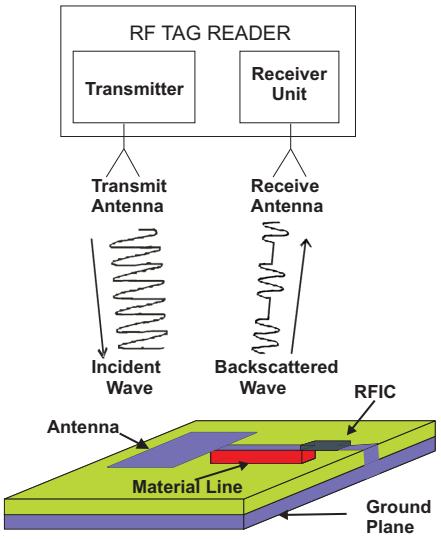

Fig. 1. Components of a REMS Sensor.

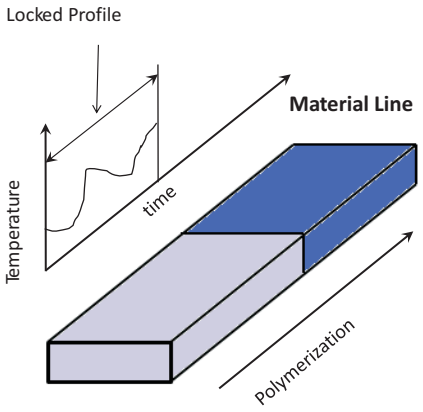

Fig. 2. The polymerization process records the historical temperature profile in the spatial distribution of electrical properties of the material line.

section III. Two proof-of-concept structures are investigated as possible implementations. The first is a three section lossless material line, discussed in section IV. For practical scenarios, specially in the context of a REMS sensor, it is important to be able to extract the material properties of a dissipative electro-material line. A possible structure incorporating a monopole probe to measure the complex permittivity is described in section V, followed by the discussion and conclusion in section VI. Our previous work includes a study of the feasibility of the REMS sensing concept [18]. That study, which was limited to lossless materials, is reviewed below. The present work extends that research to lossy materials.

II. REMS Sensing Concept

A REMS sensor consists of three distinct components working together to provide the capability to passively sense environmental information. The first component is the electro-material line, a chemical strip sandwiched between the ground plane and top trace of an RF tag's microstrip transmission line. The second component, the reflector circuitry, consists of the transmission line itself, the radio-frequency integrated circuit (RFIC) that performs backscatter and identification functions, and any RF tag antennas. Finally, an RF reader must be used to interrogate the REMS sensor as well as perform the signal processing for data extraction. These components are illustrated in Fig. 1. Conceivably, the REMS concept could be implemented with existing UHF or microwave passive RFID integrated circuits, greatly lowering cost and allowing passive interrogation of the sensor. In a conventional backscatter RFID system, the signal is reflected from a binary-switched load, providing two potential frequency-dependent measurements for extracting material line parameters [19]. Since an RFID reader filters out unmodulated scatter components, an RFID-based REMS sensor would allow a much more precise measurement compared to other forms of remote sensing.

Any material that has environmental sensitivity to permeability, permittivity, or conductivity may be a candidate for the electro-material line in the REMS sensor. For example, a simple instantaneous temperature sensor could incorporate thermotropic liquid crystals. These types of liquid crystals experience state disordering upon heating, leading to a change in their electrical (and optical) properties [20], [21]. Another candidate material may be a line substrate doped with ferroelectric or super-paramagnetic particles [22]. Such a device could use the nonlinear relationship between field and flux density components to sense external field strengths. Our immediate interest in REMS is to sense the electrical properties of thermotropic liquid crystals (LCs) trapped in a polymer substrate to record the temperature data. As the temperature changes with time, the polymerization process through the material line records the historical temperature profile in the spatial distribution of the electrical properties. One such material line is shown in Fig. 2.

The REMS sensor concept may also allow for materials that time-record other environmental attributes, thus providing a form of chemical memory rather than electrical memory that would achieve a completely passive sensor. This type of sensor functionality cannot be achieved under today's 'system on a chip' paradigm, which still requires external power supplies for electronic memory recording functions.

The REMS concept was demonstrated in a recent study [18], where the sensor is modeled using three cascaded microstrip transmission lines (Fig. 3), each with a different substrate material acting as three wells of sensor material. The line is terminated in a resistive load which causes part of the incident wave to be absorbed and part reflected back to the input port. For the frequency range of 1-5 GHz, the relative permittivity, ϵ_r, of each segment was swept across a range of values, and the values of reflection coefficient, Γ_{IN}, at the input of the system were computed. Each transmission line acts as a two port network, and the complete system of the cascaded lines can be analyzed in terms of S-parameters and signal flow graphs using Eq. 1 [23].

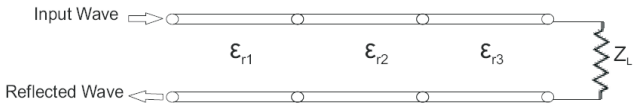

Fig. 3. The microstrip line model with three discrete segments, having different permittivity profiles, terminated in a load to emulate a REMS sensor with three wells of sensor material.

$$\Gamma_{IN} = S_{11} + \frac{S_{12}S_{21}\Gamma_L}{1 - S_{22}\Gamma_L} \tag{1}$$

Our goal is to reconstruct the spatially distributed permittivity profile. The complex-valued reflection coefficient contains magnitude and phase information, and RFID readers perform fully coherent detection and recover both [24]. In our system, both the phase and the magnitude are used by the inversion algorithm. To demonstrate that the response to slight perturbations in the permittivity profile is substantial, the dielectric constant of the second bin in Fig. 3 was changed for four different values, and the reflection coefficient was calculated for each case. The effect on Γ_{in}, for four values of ϵ_{r2}, with $\epsilon_{r1} = 2.5$ and $\epsilon_{r3} = 3.5$, is shown in Fig. 4. Theoretically, every material profile will produce a unique frequency sweep, although designing a wide range of switchable loads (Z_A, Z_B, and possibly more) will greatly affect measurement resolution and sensitivity. The amount of power backscattered depends on the impedance mismatch between the antenna and the material line terminated in Z_A or Z_B. The corresponding reflection coefficients, Γ_A and Γ_B, determine how much power is available to power up the RFIC and how much is backscattered.

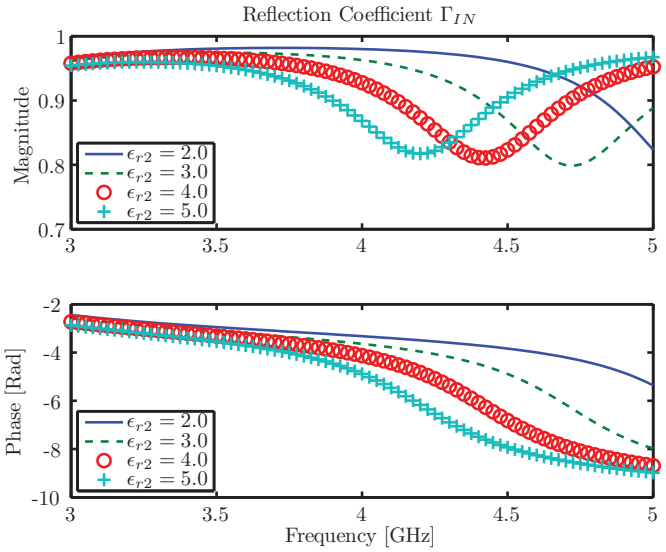

Fig. 4. Phase and magnitude of Γ_{IN} for $\epsilon_{r2} = 2$, 3, 4 and 5, calculated from the signal flow graph.

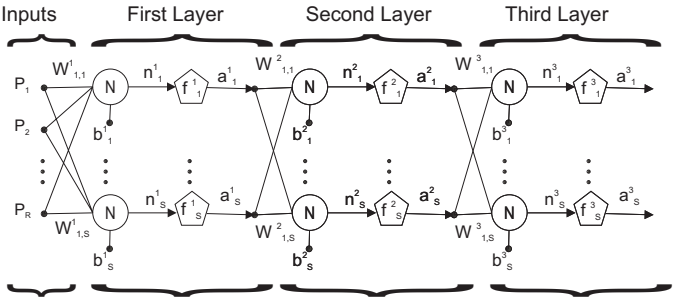

Fig. 5. Three layers of multiple neurons.

III. Neural Networks

The idea of neural networks evolved in the late 19th century in an attempt to understand how the human brain functions. The concept of decentralized network units (neurons) was introduced in 1943 when McCulloch and Pitts developed the first mathematical model of a neuron [25]. Inspired from brain function, the neural network is generally used to solve artificial intelligence problems without requiring a model of the system. Neural networks are adjusted and trained to solve the problems that are difficult to solve using conventional techniques and are extremely useful in pattern recognition and function approximation problems.

In a typical single neuron having a scalar input p, p is multiplied with a weight w and added to a bias/offset b. The output forms the argument of an activation function (transfer function) f, whose output a is the output of the neuron. The activation function is chosen by the designer, while the weight and bias (if used) are adjusted by some learning rule [26]. The output function is described by Eq. 2.

$$a = f(wp + b) \tag{2}$$

For many systems, one neuron is insufficient and therefore multiple neurons and multiple neuron layers are used, as depicted in Fig. 5. For one such layer comprising S neurons, there may be an arbitrary number of inputs R, each connected to all S neurons. The resulting weight matrix has dimension $S \times R$. The number of neurons is independent of the number of rows and columns [26]. All neurons usually have the same transfer function, although this is not always the case [26]. In the event that one layer of multiple neurons is inadequate, a network with additional (hidden) layers can be used. Each layer has its own weight matrix W, bias vector b, net input vector n, and output vector a. For R inputs and S^1 neurons in the first layer, the second layer can be considered as a layer with S^1 inputs, S^2 neurons and a weight matrix of order $S^1 \times S^2$. The input to the second layer is a^1 and its output is the input to the next layer.

The final output, a^3, is given by Eq. 3.

$$a^3 = f^3(W^3 f^2(W^2 f^1(W^1 p + b^1) + b^2) + b^3) \tag{3}$$

The transfer function may be linear or non-linear depending upon the problem. We use the logsigmoidal transfer function,

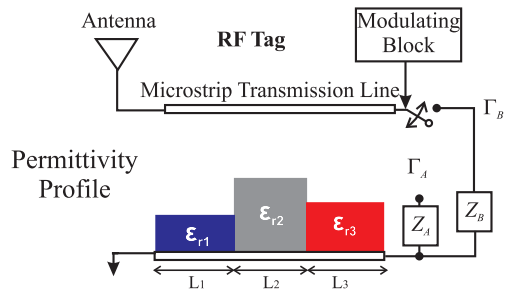

Fig. 6. The backscatter setup having 3-step micorstripline emulating a 3-bin electro-material line

which takes an input from minus infinity to plus infinity and compresses the output into the range 0 to 1 according to the expression in Eq. 4.

$$a = \frac{1}{1+e^{-n}} \tag{4}$$

The training algorithm must minimize the errors between the desired and the actual network outputs as quickly as possible. A variety of heuristic or numerical optimization algorithms are reported in the literature [26], [27], [28], [29], [30], [31]. Our preliminary investigation suggested that the Levenberg Marquardt (LM) algorithm exhibited superior performance in terms of absolute average error and the computation time [18]. The algorithm was designed to approach second order training speed without computing the Hessian H, instead using the approximation $H = J^T J$, where J is the Jacobian containing the first derivative of network errors with respect to weights and biases. The gradient is computed as $g = J^T e$, where e is the vector of network errors [32]. The Jacobian is computed through a standard back-propagation technique which is much less complex then computing the Hessian [33]. The algorithm may be written as

$$x_{k+1} = x_k - [J^T J + \mu I]^{-1} J^T e \tag{5}$$

IV. REMS Sensor for Lossless Material Line

As a first step for using neural networks in the REMS sensor application, a feasibility study was carried out for a lossless material line [18]. Training data were generated by computing Γ_{in} for cascaded microstrip lines, emulating three bins of the electro-material line as shown in Fig. 6, where Z_A and Z_B denote the switchable loads at the input port of the RFIC. For the purpose of training and then testing and validating, the magnitude and phase of reflection coefficient were organized in the data matrix D, which has the form shown in Eq. 6.

$$D = \begin{bmatrix} |\Gamma| \\ \angle\Gamma \end{bmatrix} \tag{6}$$

To test the methodology, the dielectric constants ϵ_{r1}, ϵ_{r2} and ϵ_{r3} were varied from 2-5 with a step size of 0.1, as the frequency was swept across the 5-6 GHz range with a step size of 100 MHz. The resulting data matrix had dimensions $22 \times 29,971$. The ANN architecture is described in Fig. 7.

The best-performing architecture was determined by carrying out simulations with single hidden layer networks of 5, 10, 15, 20 and 25 neurons, and a two layer network with 10 neurons each. The results were compared in terms of error and the coefficient of regression analysis. Each network was tested for a range of permittivity values. A single layer with 20 neurons appeared to produce the best absolute mean error and computation efficiency, even in the presence of white Gaussian noise [18]. The $\%$ errors for 20 neurons in the absence of noise are shown in matrix $\%E_{20}$ in Eq. 7.

$$\%E_{20} = \begin{bmatrix} 4.6\% & 1.04\% & 0.14\% \\ 1.37\% & 0.11\% & 0.5\% \\ 0.30\% & 0.17\% & 0.23\% \end{bmatrix} \tag{7}$$

The REMS sensor was further validated experimentally, using a device with three microstrip transmission lines cascaded together. Each microstrip line was 1.25cm long and 0.5cm wide, with the substrate height of approximately 0.13cm. Materials with parameter values of $\epsilon_{r1} = \epsilon_{r3} = 6.15$ and $\epsilon_{r2} = 2.2$ were used. The microstrip line was terminated in a 50Ω load.

For training purposes, simulation data were generated for ϵ_{r1} and ϵ_{r3} swept across the range from 5 - 8, and for ϵ_{r2} from 1.1 - 3.6. A neural network containing a single hidden layer of 20 neurons was trained with data containing white Gaussian noise (10dB SNR). A network analyzer was then used to record S-parameters over the frequency range 1.0-2.5 GHz, and these were used as input to the ANN. To ensure that the algorithm converged to the global minimum, the neural network was tested three times with different starting weights each time. The three sets of results are tabulated in Table I. These results exhibit an average absolute error range of ± 0.6 and a coefficient of regression, R, greater than 0.92. The % error in the center bin (Trans Line 2) is comparatively higher as compared to the % error in the estimated permittivities of lines 1 and 3. However, the absolute error in the estimated relative dielectric constant of each section of the transmission line remains around ± 0.6. The increased % error in the center bin is a consequence of the lower value of ϵ_{r2} in comparison

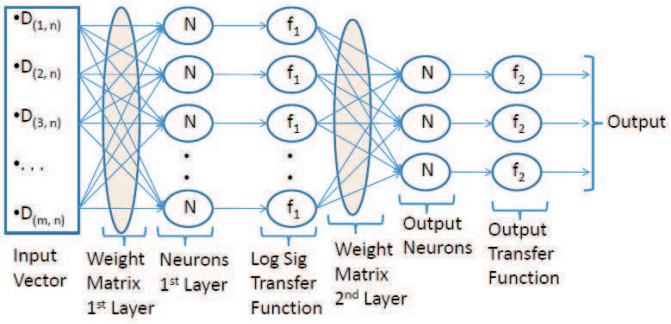

Fig. 7. ANN architecture for backsolving permittivity profile of a microstrip line structure emulating a 3-bin electro-material line

to the others. Additional results and discussion of this sensor prototype may be found in [18].

V. Reconstructing Complex Permittivity

The electrical properties of materials are characterized by the complex permittivity ϵ, which describes the interaction of a material with an applied electric field. The *relative complex permittivity* is a dimensionless quantity defined by

$$\epsilon_r = \epsilon_r^{'} - j\epsilon_r^{''} \tag{8}$$

where $\epsilon_r^{'}$ is the real part and $\epsilon_r^{''}$ is the imaginary part.

The real part of permittivity ($\epsilon_r^{'}$) is related to energy storage and the imaginary part ($\epsilon_r^{''}$) to dissipation. For most substrates, microstrip lines have a very low loss tangent and may be approximated as lossless. However, in liquids, $\epsilon_r^{''}$ can be as high as $\epsilon_r^{'}$. For a REMS sensor electro-material line that relies on the spatially distributed electrical properties of thermotropic liquid crystals, it is important to extend the neural network based methodology to extracting the complex material properties. Different resonant and non-resonant methods have been reported in the literature for measuring the complex permittivity of materials [34]. The input impedance of a monopole probe immersed in an approximately semi-infinite dielectric medium may be used to determine the complex permittivity of the medium [35]. Based on the rigorous expression for the impedances of monopole antennas in half space [36], various *in-situ* procedures are reported in the literature for extracting complex permittivities [37], [38], [39].

To better understand the thermo-responsive nature of materials at microwave frequencies, a nematic liquid crystal *4-Cyano-4 Pentylbiphenyl*, commonly known as *5CB*, was studied using a monopole probe. *5CB* is a nematic liquid crystal which undergoes a phase transition from a crystalline state to nematic state at 18^oC and it goes from nematic to an isotropic state at 35^oC. To observe the thermo-responsiveness, a 10mm long monopole probe was immersed in *5CB*, and S11 measurements were recorded using a vector network analyzer for temperatures varying from 19.8^oC to 25.7^oC. The results are shown in Fig. 8.

A noticeable change is observed in S11 measurements recorded for the frequency range from 2 - 5 GHz, suggesting the possibility of sensing temperature variations as small as approximately 2^oC. Similar thermotropic behavior was observed for Isopropyl Alcohol when temperature was varied from 9.7^oC to 36.9^oC. S11 measurements of a monopole probe immersed in Isopropyl Alcohol are shown in Fig. 9. This leads to the next step of developing a methodology to extract the complex permittivity of the material using a scheme applicable on the REMS sensor.

Our previous work, shows that neural networks can be used to reconstruct the permittivity profile of lossless stratified medium from the complex reflection coefficient [18]. For a dissipative medium, the complex-valued nature of the permittivity makes the problem incompatible with conventional neural networks, which are designed to process real-valued

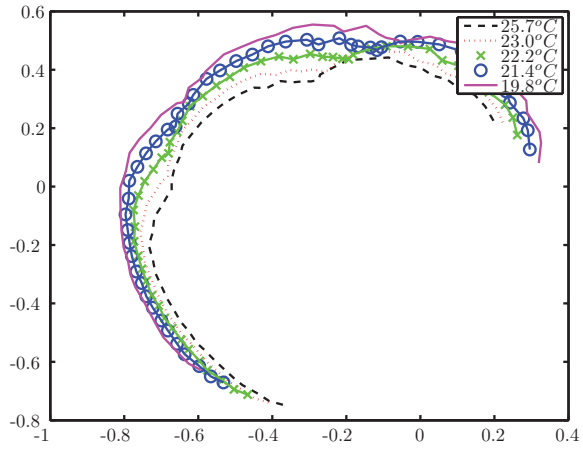

Fig. 8. Measured S11 for a 10mm monopole probe immersed in the liquid crystal 5CB. The real part is plotted on the horizontal axis and the imaginary part on the vertical.

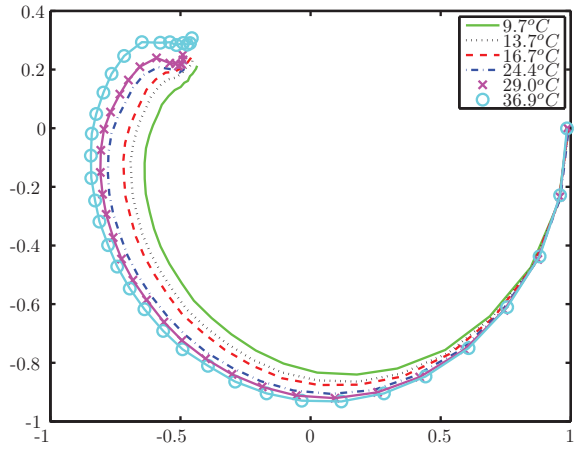

Fig. 9. Measured S11 for a 10mm monopole probe immersed in Isopropyl Alcohol.

data. One possible approach is to use a complex valued back propagation neural network, which might result in better accuracy, but these are considered more difficult to implement [40]. Another possible approach is to split the network into two networks, one dealing with the real part and the other dealing with the imaginary part (with both using real valued input data). Such an approach, for a broad-band evaluation of complex permittivity, employed the finite difference time domain technique to generate training data [41]. However, this approach has limitations such as the loss of correlation between the real and imaginary parts of the complex input data [42]. In fact, there is usually considerable correlation between the real and imaginary parts of the complex data, which can not be effectively utilized if real and imaginary values of data are manipulated independently [43].

Here we propose a different approach to serve as a proof-of-concept for a lossy REMS sensor. We use a monopole probe embedded in a lossy medium in conjunction with two back-propagation neural networks to reconstruct the complex

TABLE I
THE ACTUAL VALUES OF $\epsilon_{r1,2,3}$ COMPARED TO THE VALUES ESTIMATED USING NEURAL NETWORKS FOR THE FREQUENCY RANGE 1-2.5 GHZ.

	Trans Line 1 ϵ_{r1}	Trans Line 2 ϵ_{r2}	Trans Line 3 ϵ_{r3}	Average Error $(\epsilon_{rn} - \epsilon_{rne})$
Target Value (ϵ_{rn})	6.15	2.20	6.15	
Estimate 1 (ϵ_{rne})	5.72	2.73	5.60	
% Error	6.9%	24%	8.9%	13.2%
Estimate 2 (ϵ_{rne})	5.72	2.89	5.53	
% Error	6.9%	31%	10.1%	15.9%
Estimate 3 (ϵ_{rne})	5.67	2.81	5.69	
% Error	7.8%	27.7%	7.47%	14.3%

permittivity of dissipative media. In contrast to using real and imaginary parts separately, the phase and magnitude of complex reflection coefficient are used as inputs to each of the two networks, one of which one solves for the real part while the other solves for the imaginary part of the complex permittivity.

Neural networks can be trained to reconstruct the complex permittivity either for $\epsilon_r^{'}$ and $\epsilon_r^{''}$, or for $|\epsilon_r|$ and $\angle\epsilon_r$. Our choice for the network outputs is based on the reason that permittivity is almost always described in terms of real and imaginary parts ($\epsilon_r = \epsilon_r^{'} - j\epsilon_r^{''}$), and that can be more easily interpreted in terms of the physics of materials.

The construction of an ANN requires (i) training data, (ii) a training algorithm, and (iii) an ANN architecture. In this part, the ANN uses analytical data generated for a monopole probe according to the model presented in [36]. Following our previous work, we use the Levenberg Marquardt backpropagation algorithm [18]. The architecture includes one hidden layer, with number of neurons selected by trial and error.

The proposed system uses a monopole probe with a ground plane, immersed in the dielectric medium, and connected to a Vector Network Analyzer (VNA). The monopole probe geometry is shown in Fig. 10, where h is the height and a is the radius of the probe, while d is the diameter of the ground plane. The VNA is used to obtain the reflection coefficient of the probe through $S11$ measurements across the frequency range from 2.5 to 5 GHz. The reflection coefficient is related to the input impedance of the probe through the simple relationship given by Eq. 9.

$$\Gamma = \frac{Z_{in} - Z_o}{Z_{in} + Z_o} \tag{9}$$

In Eq. 9, Γ is the complex reflection coefficient, Z_{in} is the input impedance of the monopole probe, and Z_o is the characteristic impedance of the coaxial cable connected to the probe, which in this case is 50Ω. The input impedance Z_{in} is computed using rigorous expression developed by Wu [36], and is given by

$$Z_{in}^{*} = \frac{\omega\mu_o}{j4k(S + CU)} \tag{10}$$

where

$$k = \beta + j\alpha = \omega\left[\mu\left(\epsilon^{'} - j\epsilon^{''}\right)\right]^{1/2} \tag{11}$$

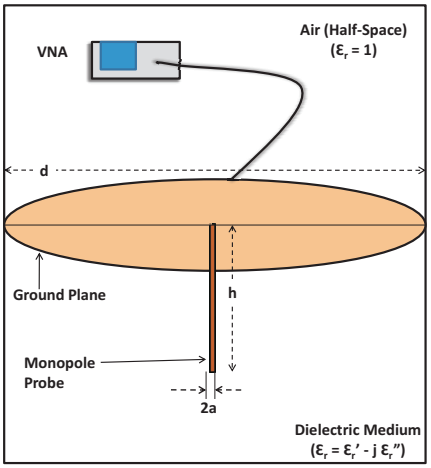

Fig. 10. A monopole probe of height h and radius a, immersed in a dissipative dielectric medium with permittivity $\epsilon_r = \epsilon_r^{'} - j\epsilon_r^{''}$, and connected to VNA

The functions S, C and U, along with the approximations inherent in these expressions, are described in detail in *Appendix A* of [37]. These functions along with k depend on the measurement frequency, the geometrical dimensions of the monopole probe (height and radius), and the dielectric properties of the medium ($\epsilon_r = \epsilon_r^{'} - j\epsilon_r^{''}$).

The validity of the monopole probe model is limited to a specific frequency range depending upon the ratio h/λ. For a $10mm$ long probe, values of relative permittivity ranging from 3 - 10 correspond to resonant frequencies ranging from 4.5 GHz to 2.76 GHz, respectively. The phase and magnitude response to a change in complex permittivity is more pronounced close to the resonance and therefore, our use of this model is limited to the frequency range from 4 to 5 GHz for the real part of complex permittivity ranging from 3 - 6. The other factor which limits the capability of model is determined by the loss tangent of the medium. It was observed that the model only worked well for values of $\tan\delta \leq 0.2$ and consequently we restrict the values of $\epsilon_r^{''}$ to the range from 0 to 0.5 when the smallest value of $\epsilon_r^{'}$ is 3.0.

The magnitude and phase of the reflection coefficient was initially combined into a single vector of training data as illustrated in the matrix D shown in Eq. 6. The ANN performance was adequate for noise free data, however it was observed to be sensitive to the presence of measurement noise. Measurement

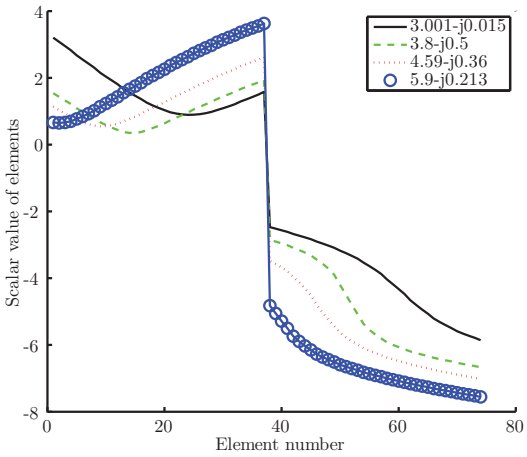

Fig. 11. Scaled input vectors corresponding to different values of complex permittivity $\epsilon_r = \epsilon_r^{'} - j\epsilon_r^{''}$

noise was simulated by adding white Gaussian noise, and a proportionally larger error was observed in the estimated values of $\epsilon_r^{''}$ as the noise was increased. These simulations motivated the incorporation of a scale factor into the algorithm, so the data matrix D was modified to D_{sc} by scaling the magnitude of reflection coefficient by a factor N as shown in Eq. 12.

$$D_{sc} = \begin{bmatrix} N \times |\Gamma| \\ \angle\Gamma \end{bmatrix} \tag{12}$$

An appropriate value of the scaling factor was observed to be $N \approx 6$. Several vectors from D_{sc} corresponding to different values of complex ϵ_r are shown in Fig. 11.

Two separate networks are employed using the complex reflection coefficient as the input in the form described in Eq. 12. By trial and error we determined that a network with one hidden layer of 25 neurons gave superior performance in terms of mean square error. Despite having the same input training data and neuron layer architecture, the networks differ in terms of weights matrices since they are tracking different outputs. The two outputs are combined together to reconstruct the complex permittivity as shown in Fig. 12. In the figure, $|\Gamma_{fn}|$ and $\angle\Gamma_{fn}$ indicate the magnitude and phase of input reflection coefficient computed/measured at frequency f_n. The complete frequency range of interest is divided into n steps.

The real part of complex permittivity ($\epsilon_r^{'}$) was swept from 3.0 to 6.0 with an increment of 0.025, while the imaginary part ($\epsilon_r^{''}$) was swept from 0 to 0.5 with a step size of 0.005. Measurement noise was simulated by adding white Gaussian noise with 10dB SNR to the training data and then same proportion of noise was induced in the test data as well. The network was then tested for 231 different values of ϵ_r that were not used for training the network. The results, tabulated in Table II, were found to exhibit an error less than 4%. To confirm that network has converged to a global minimum and not a local minimum, we repeated the simulation several times and observed the results for consistency, following [26].

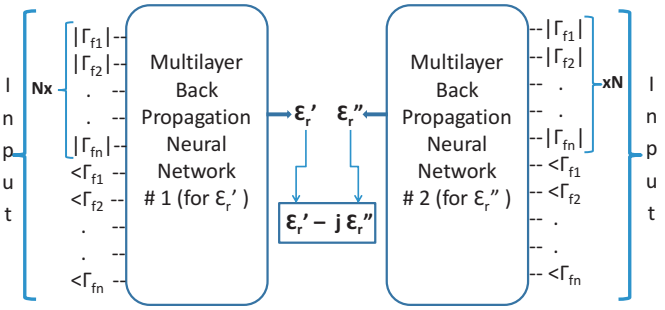

Fig. 12. Neural network model comprising two networks using 1 hidden layer each, with #1 solving for $\epsilon_r^{'}$ and #2 reconstructing $\epsilon_r^{''}$ using the Levenberg Marquardt back-propagation algorithm

VI. Discussion and Conclusion

We propose the concept of a passive REMS sensor, with the potential capability of extracting the time profile of an environmental variable such as temperature. For lossless sensors, a single neural network was previously demonstrated to successfully determine the spatially distributed permittivity profile from the reflection coefficient collected over a range of frequencies. Since an electro-material line constructed with thermotropic liquid crystals will be lossy, this paper proposes an extension of the approach to handle complex permittivity profiles. We consider the use of two neural networks, each using the Levenberg Marquardt back-propagation algorithm, with one solving for the real part while the other solves for the imaginary part. Both networks require one hidden layer with 25 neurons. Scaling has been applied to the input vectors to improve the robustness against measurement noise. The complex permittivity extraction process was demonstrated using a single lossy medium and a monopole probe. The complex permittivity estimated using this approach exhibited less than 4% error in the presence of white Gaussian noise (10dB SNR).

The success of the complex permittivity extraction suggests that the approach can be extended to handle a spatially distributed lossy profile, which we leave to future work. We acknowledge that our particular implementation currently requires a minimum bandwidth of about 1 GHz to accurately estimate the permittivity profile, which eliminates the possibility of using the ISM band at 5.8 GHz. However, passive ultrawide bandwidth (UWB) RFID systems are under consideration for the next generation RFID [44], and our approach may be practical for such a system.

References

[1] A. Mita and S. Takahira, "Damage index sensor for smart structures," *Structural Engineering and Mechanics*, vol. 17, no. 3-4, pp. 231–346, 2004.

[2] J. T. Simonen, M. M. Andringa, K. M. Grizzle, S. L. Wood, and D. P. Neikirk, "Wireless sensors for monitoring corrosion in reinforced concrete members," *Proceeding of SPIE - Smart Structires and Materials*, vol. 5391, pp. 587–596, 2004.

[3] K. J. Loh, J. P. Lynch, and N. A. Kotov, "Passive wireless sensing using swnt-based multifunctional thin film patches," *International Journal of Applied Electromagnetics*, vol. 28, pp. 87–94, 2008.

TABLE II
COMPARISON OF ACTUAL VALUES OF $\epsilon_r = \epsilon_r^{'} - j\epsilon_r^{''}$ VS TWO SETS OF ESTIMATED VALUES AND THE RESPECTIVE PERCENT ERROR FOR FREQUENCY RANGE 4 -5GHZ

Actual Values	NN Output(Set1)	% Error	NN Output(Set2)	% Error
3.01 - j0.015	3.1092 - 0.1149i	1.17	3.1570 - 0.1273i	1.97
4.59 - j0.36	4.6174 - 0.3403i	0.73	4.5729 - 0.2114i	3.24
5.27 - j0.213	5.0794 - 0.2960i	3.94	5.2315 - 0.2461i	0.96
5.9 - j0.5	5.5745 - 0.3278i	3.06	5.7088 - 0.4846i	0.62

[4] G. Marrocco and D. Scarana, "Permittivity passive rfid sensor for non-cooperating objects," in *The Second European Conference on Antennas and Propagation, EuCAP*, 2007, pp. 1 – 4.

[5] G. Marrocco and F. Amato, "Self-sensing passive rfid: From theory to tag design and experimentation," in *European Microwave Conference, EuMC*, Oct. 2009, pp. 1 – 4.

[6] R. Bhattacharyya, C. Floerkemeier, and S. Sarma, "Low-cost, ubiquitous rfid-tag-antenna-based sensing," *Proceedings of the IEEE*, vol. 98, no. 9, pp. 1593 –1600, 2010.

[7] G. Durgin, "Reflected Electro-Material Signature (REMS) Sensor," Provisional Patent filed on June 2008.

[8] C. Q. Lee, "Wave propagation and profile inversion in lossy inhomogeneous media," *Procedings of the IEEE*, vol. 70, no. 3, pp. 219–228, Mar. 1983.

[9] H. W. Yang and R. S. Chen, "Fdtd analysis on the effect of plasma parameters on the reflection coefficient of the electromagnetic wave," *Optical and Quantum Electronics*, vol. 39, no. 15, pp. 1245–1252, Dec. 2007.

[10] E. Kemppinen, "Effective permittivity and attenuation coefficient of microstrip transmission line determined by 1-port and 2-port measuring methods," *Measurement Science and Technology*, vol. 11, pp. 38–44, 2000.

[11] Q. J. Zhang, K. C. Gupta, and V. K. Devabhaktuni, "Artificial neural networks for rf and microwave design - from theory to practice," *IEEE Transactions on Microwave Theory and Techniques*, vol. 51, no. 4, pp. 1339–1350, Apr. 2003.

[12] H. Kabir, M. Yu, and Q. J. Zhang, "Recent advances of neural network-based em-cad," *International Journal of RF and Microwave CAE*, vol. 20, pp. 502–511, Jul. 2010.

[13] S. R. H. Hoole, "Artificial neural networks in the solution of inverse electromagnetic field problems," *IEEE Trans. on Magnetics*, vol. 29, no. 2, pp. 1931–1934, Mar. 1993.

[14] I. Elshafiey, L. Udpa, and S. S. Udpa, "Application of Neural Networks to Inverse Problems in Electromagnetics," *IEEE Trans. on Magnetics*, vol. 30, no. 5, pp. 3629–3632, Sep. 1994.

[15] F. Yaman and S. Simsek, "Neural network approach to determine nonsmooth one-dimensional profiles in inverse scattering theory ," *Microwave and Optical Technology Letters*, vol. 49, no. 12, pp. 3158–3162, Sep. 2007.

[16] C. Christodoulou and M. Georgiopoulos, *Application of Neural Networks in Electromagnetics*. Boston, London: Artech House, 2001.

[17] W. Sha and K. Edwards, "The use of artificial neural networks in materials science based research," *Materials and Design*, vol. 28, no. 6, pp. 1747 – 1752, 2007.

[18] A. Hasan, A. F. Peterson, and G. D. Durgin, "Feasibility of passive wireless sensors based on reflected electro-material signatures," *The Applied Computational Electromagnetic Society Journal*, vol. 25, no. 10, pp. 552–560, Jun. 2010.

[19] J. Griffin and G. Durgin, "Complete link budgets for backscatter-radio and rfid systems," *Antennas and Propagation Magazine, IEEE*, vol. 51, no. 2, pp. 11 –25, Apr. 2009.

[20] S. Chandrasekhar, *Liquid Crystals, 2nd Ed.* Cambridge: Cambridge University Press, 1992.

[21] P. Collings and M. Hird, *Introduction to Liquid Crystals*. Bristol, PA: Taylor & Francis, 1997.

[22] R. O'Handley, *Magnetic Materials: Principles and Applications*. Wiley-Interscience, 1999.

[23] D. M.Pozar, *Microwave Engineering , 3rd Ed*, John Wiley and Sons-New York, 2005.

[24] P. Nikitin, R. Martinez, S. Ramamurthy, H. Leland, G. Spiess, and K. Rao, "Phase based spatial identification of uhf rfid tags," in *2010 IEEE International Conference on RFID*, 2010, pp. 102 –109.

[25] K. Mehrotra, S. Ranka, and C. K. Mohan, *Elements of Artificial Neural Networks*. MIT Press, 1996.

[26] M. T. Hagan, H. B. Demuth, and M. Beale, *Neural Network Design*. Boston, MA: PWS Publishing Company, 1996.

[27] D. G. Luenberger, *Introduction to Linear and Non Linear Programming*. Addison Wesley Pub. Co., 1973.

[28] M. Powell, "Restart procedures for the conjugate gradient method," *Mathematical Programming*, vol. 12, pp. 241–254, 1977.

[29] E. Beale, *"A derivation of conjugate gradients" in F.A.Lootsma, Ed., Numerical methods for nonlinear optimization*. London Academic Press, 1972.

[30] M. Moller, "A scaled conjugate gradient algorithm for fast supervised learning," *Neural Networks*, vol. 6, pp. 525–533, 1993.

[31] R. Battiti, "First- and Second-Order Methods for Learning: Between Steepest Descent and Newton's Method ," *Neural computation*, vol. 4, no. 2, pp. 141–166, Jun. 1992.

[32] D. W. Marquardt, "An Algorithm for Least-Squares Estimation of Nonlinear Parameters," *Journal of the Society for Industrial and Applied Mathematics*, vol. 11, no. 2, pp. 431–441, Jun. 1963.

[33] M. Hagan and M. Menhaj, "Training feed-forward networks with the Marquardt algorithm," *IEEE Transactions on Neural Networks*, vol. 5, no. 61, pp. 989–993, Nov. 1994.

[34] L. F. Chen, C. K. Ong, C. P. Neo, V. V. Varadan, and V. K. Varadan, *Microwave Electronics Measurements and Material Characterization*. West Sussex, England: John Wiley & Sons, 2004.

[35] G. S. Smith and J. D. Nordgard, "Measurement of the electrical constitutive parameters of materials using antennas," *IEEE Transactions on Antennas and Propagation*, vol. AP-33, no. 7, pp. 783–792, 1985.

[36] D. W. Gooch, J. C. W. Harrison, R. W. P. King, and T. T. Wu, "Impedances of long antennas in air and in dissipative media," *Journal of Research at the National Bureau of Standards*, vol. 67D, no. 3, pp. 355–360, May 1963.

[37] S. C. Olson and M. F. Iskander, "A new in-situ procedure for measuring the dielectric properties of low permittivity materials," *IEEE Transactions on Instrumentation and Measurement*, vol. IM-35, no. 1, pp. 2–6, Mar. 1986.

[38] A. Denoth, "The monopole-antenna : A practical snow and soil wetness sensor," *IEEE Transactions on Geoscience and Remote Sensing*, vol. 35, no. 5, pp. 1371–1375, Sep. 1997.

[39] F. M. Sagnard, V. Guilbert, and C. Fauchard, "In-situ characterization of soil moisture content using a monopole probe," *Journal of Applied Geophysics*, vol. 68, pp. 182–193, 2009.

[40] A. Hirose, *Complex-Valued Neural Networks*. Berlin / Heidelberg: Springer, 2006.

[41] H. Acikgoz, Y. L. Bihan, O. Meyer, and L. Pichon, "Neural networks for broad-band evaluation of complex permittivity using a coaxial discontinuity," *Eur. Phys. J. Appl. Phys.*, vol. 39, no. 2, pp. 197–201, 2007. [Online]. Available: http://dx.doi.org/10.1051/epjap:2007073

[42] G. M. Georgiou and C. Koutsougeras, "Complex domain bakpropagatoin," *IEEE Transactions on Circuits and Systems - II: Analog and Diital Signal Processing*, vol. 39, no. 5, pp. 330–334, May 1992.

[43] M. Smith and Y. Hui, "A data extrapolation algorithm using a complex domain neural network," *IEEE Transactions on Circuits and Systems - II: Analog and Diital Signal Processing*, vol. 44, no. 2, pp. 143 –147, Feb 1997.

[44] D. Dardari and R. D'Errico, "Passive ultrawide bandwidth rfid," in *Global Telecommunications Conference, 2008. IEEE GLOBECOM 2008. IEEE*, 30 2008.